

The influence of the addition of carbon spheres on photoactivity of TiO₂ and ZnO in CO₂ reduction process

Antoni W. Morawski, Katarzyna Ćmielewska^{*}, Ewelina Kusiak-Nejman, Piotr Staciwa, Joanna Kapica-Kozar, Ewa Ekiert, Iwona Petech, Urszula Narkiewicz

Department of Inorganic Chemical Technology and Environment Engineering, Faculty of Chemical Technology and Engineering, West Pomeranian University of Technology in Szczecin, Pułaskiego 10, 70-322 Szczecin, Poland

ARTICLE INFO

Keywords:

Photocatalysis
Carbon spheres
Titanium dioxide
Zinc oxide
Carbon dioxide

ABSTRACT

The development of an effective photocatalyst for CO₂ reduction is currently being addressed by many scientists. This study concerns the influence of the addition of carbon spheres (CS) on photoactivity of TiO₂ and ZnO. The photocatalysts were tested in a liquid phase system in an alkaline environment. The suspensions of the tested materials were irradiated with UV–Vis light for 6 h. Then, the amount of the obtained products in the gas phase was analysed by gas chromatography. The identified products of CO₂ photoreduction were hydrogen, carbon monoxide, and methane. Based on the results, it was found that CS/TiO₂ and CS/ZnO showed similar activity in carbon dioxide reduction processes, however, more product amounts were obtained in experiments with the use of CS/TiO₂ materials. The addition of carbon spheres to titanium dioxide improved its activity in carbon monoxide production. The maximum photoactivity of CS/TiO₂ was observed for the addition of 0.1 g of CS. On the other hand, in the case of CS/ZnO materials, carbon spheres did not positively affect their performance. Nevertheless, their activity increased with the CS amount.

1. Introduction

In the face of current dangerous climate changes, the photoreduction of CO₂ into valuable products is one of the most promising methods to protect our environment. But, at the same time, it is a very complex process influenced by many parameters. That is why scientists from all over the world are intensively studying this challenging issue.

The CO₂ molecule is thermodynamically stable [1], so any reaction with it requires a significant amount of energy. Therefore, the conditions for photocatalysis, e.g., the type of photocatalyst, its size and sorption properties, the type of system, pH, temperature, intensity and range of radiation, are crucial to achieving a high level of CO₂ reduction.

The selection of the photocatalyst plays an important role here. TiO₂ is the most commonly used in photocatalysis, not only in carbon dioxide reduction but also in organic pollutants degradation, dye bleaching, or air and water purification in general [2–7]. Its P25 type, composed of 75% anatase and 25% rutile, is highly effective for photocatalytic processes and is more active than single-phase TiO₂ [8,9]. Titanium dioxide in the form of brookite has been characterized by even higher photoactivity [10–12]. There are many publications concerning CO₂ reduction

processes in which titanium dioxide in various forms is employed [13–17].

Aside from titanium dioxide, ZnO is considered a material with similar properties. According to the literature, it has a strong electron–migration ability, high exciton binding energy, and the ability to generate electron–hole pairs rapidly [18]. Unfortunately, it has a relatively large band gap. Hence it needs to be activated with UV light [19–21]. The poor ability to absorb visible light significantly limits the application of ZnO in more economical solutions that use sunlight. It is most commonly used to remove detergents, dyes, and pesticides [22–26]. However, publications concerning CO₂ photoreduction can be found as well [27,28]. According to the literature, ZnO can also be successfully used in CO₂ electroreduction processes [29–31].

Both TiO₂ and ZnO are characterized by non-toxicity and relatively low production costs. Based on the literature, combining those two compounds is a promising method of increasing the activity in photocatalytic processes due to the synergistic effect of TiO₂ and ZnO properties required in CO₂ photoreduction [32]. Other photocatalysts studied and described in detail in the literature include carbonaceous materials (mainly g-C₃N₄ and its composites [33–35]), salts composites

^{*} Corresponding author.

E-mail address: katarzyna.przywecka@zut.edu.pl (K. Ćmielewska).

(e.g. CdS, ZnS, MoS₂ [36–41]), or Layered Double Hydroxides (LDHs) [42–44]. The main products in the photocatalytic reduction of CO₂ with the use of those materials are carbon monoxide [36–38,43,44], methane [36–40,43], hydrogen [38,44], methanol [40–42], and formic acid [33].

Another critical factor in CO₂ photoreduction is the reactor configuration and process conditions. Currently, two types of setups are widely used, namely liquid-phase reactors, which have been known and developed for decades, and gas-phase reactors, which are newer and characterized by high efficiency [45]. The main disadvantages of liquid-phase reactors include poor solubility of CO₂ solubility in water, limited mass transfer, and agglomeration of the catalyst [46,47]. This can lead to a significant reduction in photocatalytic performance. However, the undesirable effects can be minimized, especially by using circulation, constant stirring, and solvents/reduction agents other than water [45,48,49].

As mentioned above, the stability of the carbon dioxide molecule makes it difficult to carry out the photocatalytic process. In this case, it is worth considering the process in an alkaline environment. The absorption of carbon dioxide in an aqueous solution of sodium hydroxide is a recognized method of CO₂ capture described in the scientific literature [50–53]. It is also well-known that the solubility of carbon dioxide in an aqueous NaOH solution is higher than in water. This is related to the carbonate equilibria, which means that CO₂ is present in different forms depending on the pH of the solution [54]:

- dissolved CO₂/carbonate acid (H₂CO_{3(aq)}) at pH below 6.3, which is rapidly desorbed into the gas phase;
- bicarbonate ions (HCO₃[−]), which predominate at pH between 6.3 and 10.3;
- carbonate ions (CO₃^{2−}) are only present in a strongly alkaline environment at pH values above 10.3.

Carbonate and bicarbonate ions are more reactive than CO₂ itself. Moreover, OH[−] ions from NaOH solution can be hole-scavenging and form hydroxyl radicals that prevent the recombination of hole-electron pairs [55]. In another publication [56], thanks to this property, we demonstrated that more hydrogen is produced in an alkaline environment than in aqueous (neutral) conditions.

The adsorption of CO₂ is another key factor in the photoreduction process. A good CO₂ adsorption capacity means that more CO₂ molecules can participate in the reaction on the surface of the photocatalyst. During the adsorption process, a negatively charged CO₂^{δ−} molecule is formed, a crucial intermediate product in the formation of other products of the CO₂ photoreduction process [57].

Considering the above information, experiments were carried out to investigate the photocatalytic properties in the process of CO₂ reduction in the liquid phase. The tested materials consisted of TiO₂ and ZnO, known as photoactive materials, and carbon spheres (CS) with excellent CO₂ adsorption properties and high surface area (S_{BET}). The aim was to achieve a synergistic effect of photocatalysts with carbon spheres by combining the two components with specific properties and comparing the activities of the two groups of materials tested, which were CS/TiO₂ and CS/ZnO. Through this combination, we expected to achieve enhanced CO₂ adsorption, which is crucial for the photocatalytic reduction of carbon dioxide.

2. Materials and methods

2.1. Samples preparation

The following materials were used to prepare photocatalysts: P25 type TiO₂ (AEROXIDE® TiO₂ P25, Evonik Industries AG, Germany), ZnO with particle size < 100 nm (Sigma-Aldrich, USA), and carbon spheres obtained using resorcinol and formaldehyde. A detailed description of the synthesis of carbon spheres has been described in our previous publication [58]. The mixtures of titanium dioxide or zinc oxide with

carbon spheres were prepared using a microwave-assisted solvothermal reactor (Ertec, Poland), as described elsewhere [59]. The obtained materials were ground in a mortar, and then their photocatalytic properties were assessed. 0.2 M aqueous NaOH solution was prepared from reagent-grade sodium hydroxide (Avantor Performance Materials, Poland) and distilled water.

2.2. Specific surface area, total pore volume and adsorption capacity measurements

Surface properties were determined using N₂ adsorption/desorption isotherms performed on a QUADRASORB evo™ Gas Sorption automatic system (Quantachrome Instruments, Boynton Beach, FL, USA) at −196 °C. Before each adsorption experiment, samples were outgassed at 250 °C under a vacuum of 1 × 10^{−5} mbar for 12 h using a MasterPrep multi-zone flow/vacuum degasser from Quantachrome Instruments to remove adsorbed species that could intervene in the adsorption processes. The surface area (S_{BET}) was determined in the relative pressure range of 0.05–0.3 and calculated based on Brunauer–Emmett–Teller (BET) equation. The total pore volume (TPV) was calculated from the volume of nitrogen held at the highest relative pressure ($p/p_0 = 0.99$). Pore size distributions (PSD) of the samples were determined from CO₂ adsorption isotherms at 0 °C by integrating the pore volume distribution function using the NLDFT method.

Carbon dioxide adsorption isotherms at 25 °C were measured with Quadrasorb™ automatic system (Quantachrome Instruments, Boynton Beach, FL, USA) in the pressure range between 0.01 and 0.98 bar.

2.3. Zeta potential and average particle size measurements

The zeta potential of the samples was measured using Zetasizer Nano-ZS (Malvern Instruments Ltd. Malvern, UK). The measurements were performed at a pH of 6.9, corresponding to a pH in a given process environment.

The average particle size of TiO₂ and ZnO was determined using the same instrument. The measurements were carried out for samples dispersed in ultrapure water.

2.4. SEM analysis

The surface morphology of the samples was investigated with a scanning electron microscope (SEM Hitachi SU8020, Japan) with an acceleration voltage of 5.0 kV, and magnitude of 45.0k and 50.0k.

2.5. Photocatalytic process

The experiments were performed in a liquid-phase bottle-shaped reactor. The working volume of the reactor was 766 cm³. A 150 W medium-pressure mercury lamp TQ150 Z3 (Heraeus, Germany) was used in the tests. It was characterized by a wide range of UV–Vis light, with an intense peak at about 365 nm (UV–A radiation). As presented in the scheme, the lamp was placed in a quartz condenser inside the reactor, (Fig. 1). It was constantly cooled with fresh water. The reactor was placed in the thermostatic chamber to maintain a stable temperature and exclude any light sources.

The photocatalytic processes were prepared as follows: 500 cm³ of 0.2 M aqueous NaOH solution was poured into the reactor. Then 200 mg of the tested material was added. The mixture was saturated with pure CO₂ (Messer, Poland) for 16 h. Then, the system was closed, and the lamp was turned on. The suspension of the photocatalyst was constantly stirred with the use of the magnetic stirrer and the pump (flow rate of 1.6 dm³/h). The processes were performed at 20 °C and lasted for 6 h. The gas samples for analysis were collected every 1 h.

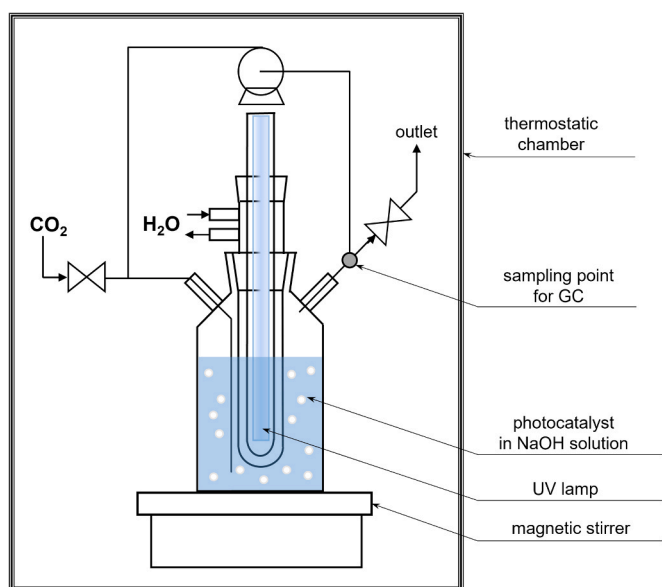


Fig. 1. Scheme of the reactor for photocatalytic process in a liquid phase.

2.6. Gas phase analysis

The gas phase composition was analyzed using a Master GC chromatograph (DANI Instruments, Italy) equipped with micropacked Shincarbon ST 100/120 column. The analyses were performed using TCD and FID detectors. The methanizer was placed between the detectors. It converted the inorganic product (carbon monoxide) to methane, allowing us to accurately determine its amount using FID. The carrier gas was argon. The volume of the analyzed gas sample was 1 cm³. The amount of hydrogen, carbon monoxide and methane in a gas phase was calculated based on the calibration curve.

3. Results and discussion

In our previously works, the textural and adsorption properties of carbon spheres and carbon spheres/metal oxides composites [59–61] were studied. In Figs. 2 and 3, CO₂ adsorption isotherms are presented for the composites based on carbon spheres and titanium dioxide and zinc oxide, respectively. It is clearly shown that together with the

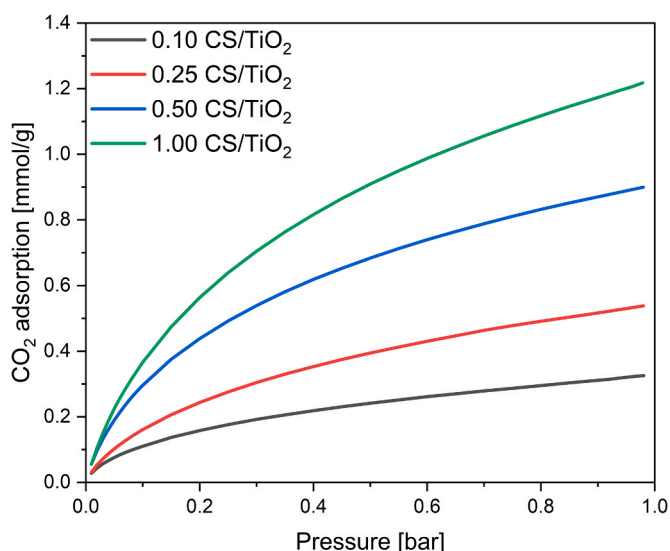


Fig. 2. CO₂ sorption isotherms of the obtained CS/TiO₂ composites.

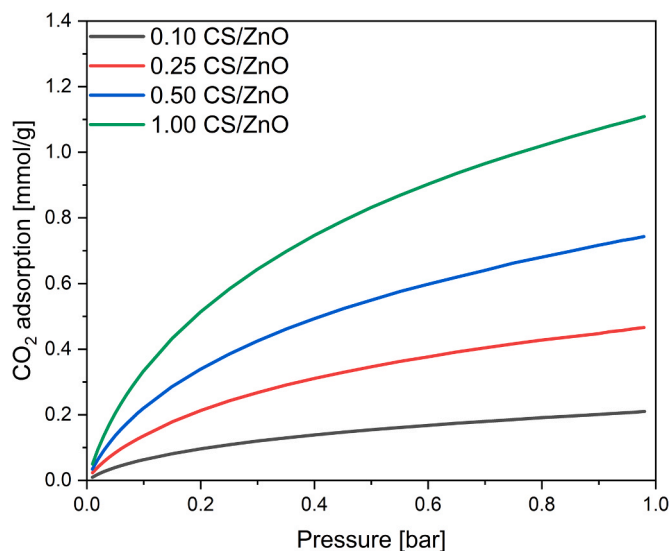


Fig. 3. CO₂ sorption isotherms of the obtained CS/ZnO composites.

increase of the carbon content in the materials higher values of CO₂ adsorption were recorded. CO₂ adsorption at 25 °C was the highest for the samples with the addition of 1.00 g of CS, and it ranged 1.22 mmol/g and 1.11 mmol/g for materials containing TiO₂ and ZnO, respectively. It was found that for all the studied samples slightly lower values of CO₂ adsorption were observed for the composites with addition of zinc oxide, regardless of the ratio of metal oxide to carbon in the obtained materials. From the available papers [62–65] it is known that in the adsorption of carbon dioxide not only the values of surface area or total pore volume is important, but above all the smallest pores, below 0.7 nm are responsible for this process. In Fig. 4 the comparison between the pore size distributions of the obtained materials is presented. It was found that the content of ultramicropores increased together with the increase of content of carbon for two types of materials. Additionally it was noticed that slightly lower volumes of micropores and ultramicropores were obtained in the case of the samples modified with zinc oxide and therefore slightly lower values of CO₂ adsorption were noticed for this type of the samples. Detailed characteristics of the textural properties of the obtained composites have been presented in the paper [59].

The experimentally determined zeta potentials at pH = 6.9 (the same

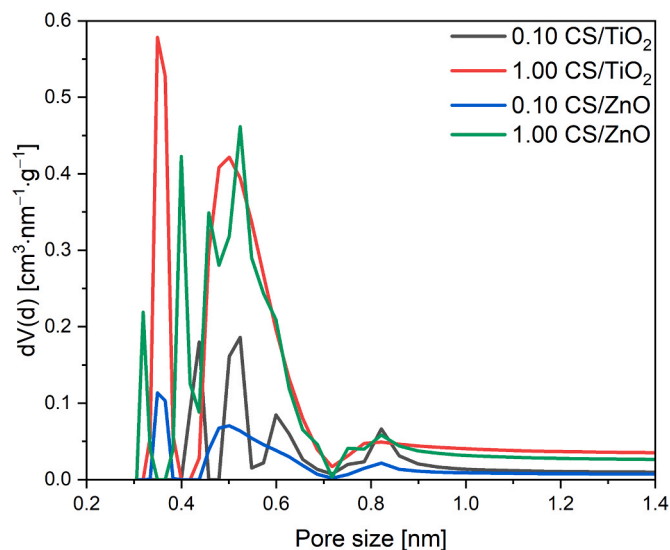


Fig. 4. Comparison of the pore size distributions of the CS/TiO₂ and CS/ZnO composites with the lowest and the highest content of carbon.

as in the photoreactor after saturation with CO₂) were negative for all base materials, and range from −9.2 mV to −19.9 mV. From the results, it can be concluded that ZnO had a less negative ζ-potential in a given environment than CS. Therefore, the repulsive forces between the particles of these two materials were weaker than in the samples containing CS and TiO₂, with the zeta potential of titanium dioxide being higher than that of carbon spheres. This could affect the transfer of electrons and also CO₂ molecules between the adsorbent and the photocatalysts. The average particle size was similar for TiO₂ and ZnO (136.2 nm and 92.5 nm, respectively), while carbon spheres were characterized by the largest value of this parameter (471.2 nm). The differences in size between an active material and the adsorbent can be seen in Fig. 5. In the SEM images shown, it can be observed that the carbon spheres are much larger in size than the photocatalysts particles. It can also be seen that TiO₂ and ZnO form agglomerates on the surface of the carbon spheres. In addition, they differ in shape. While TiO₂ is fine and rather spherical, ZnO has an elongated appearance.

The starting materials (shown in Table 1) and their mixtures with different ratios of CS to TiO₂/ZnO were tested for their photocatalytic properties in the photocatalytic reduction of CO₂ in the liquid phase, using a suspension of the tested material in a 0.2 M NaOH solution, as described in Section 2.5. It should be emphasized that the purpose of the experiments was to verify whether, after mixing materials commonly used as photocatalysts and carbon spheres with good adsorption properties and a developed specific surface area, a synergistic effect occurs and the amounts of the obtained products will be higher due to the increased ability to adsorb CO₂ and thus a longer contact time between the carbon dioxide molecule and the surface of the photocatalysts.

The CO₂ photoreduction products identified during the process are hydrogen, carbon monoxide, and methane. They can be formed in the following reactions [67–69]:

- water splitting, which is a two-electrons reaction and is the first necessary step in CO₂ reduction, hydrogen is formed:



the two-electron reduction of CO₂, leading to the formation of the main product, namely carbon monoxide:



- the eight-electron reaction that requires the most energy and produces methane:

Table 1

The selected properties of base materials [59,66].

Material	Properties				
	S _{BET} [m ² /g]	TPV [cm ³ /g]	CO ₂ 25 °C [mmol/g]	ζ-potential [mV]	Average particle size [nm]
CS	455	0.26	2.43	−13.4	471.2
P25	54	0.40	0.16	−19.9	136.2
TiO ₂					
ZnO	11	0.03	0.04	−9.2	92.5

S_{BET} – specific surface area; TPV – total pore volume; CO₂ 0 °C – CO₂ sorption capacity at 0 °C; CO₂ 25 °C – CO₂ sorption capacity at 25 °C; ζ-potential – zeta potential at pH = 6.9



These products are characterized by poor solubility in liquids and immediately desorb from the liquid phase to the gas phase after formation. Therefore, their analysis was performed only in the gas phase.

Table 2

Materials tested in photocatalytic reduction of CO₂.

Material acronym	Mass ratio of carbon spheres to TiO ₂ or ZnO	Mass of the material in the reactor [g]	Mass of pure TiO ₂ or ZnO in the reactor [g]
TiO ₂	0.00: 1.00	0.200	0.200
0.05 CS/TiO ₂	0.05: 1.00	0.204	0.194
0.10 CS/TiO ₂	0.10: 1.00	0.206	0.188
0.25 CS/TiO ₂	0.25: 1.00	0.204	0.164
0.50 CS/TiO ₂	0.50: 1.00	0.199	0.133
1.00 CS/TiO ₂	1.00: 1.00	0.203	0.102
ZnO	0.00: 1.00	0.202	0.202
0.05 CS/ZnO	0.05: 1.00	0.202	0.192
0.10 CS/ZnO	0.10: 1.00	0.201	0.183
0.25 CS/ZnO	0.25: 1.00	0.203	0.163
0.50 CS/ZnO	0.50: 1.00	0.201	0.134
1.00 CS/ZnO	1.00: 1.00	0.205	0.103

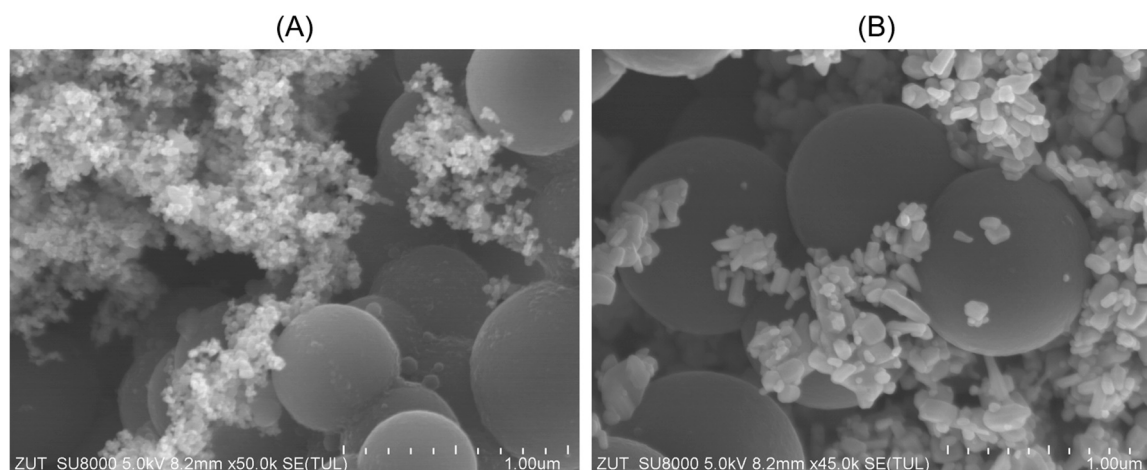


Fig. 5. SEM images of: (A) 0.50 CS/TiO₂; (B) 0.50 CS/ZnO.

The results obtained are discussed below.

The data of the tested samples are listed in Table 2. 12 experiments were performed with mixtures of TiO₂ or ZnO with carbon spheres (CS). For both groups of materials, samples were obtained with mass ratios of CS to TiO₂ or ZnO ranging from 0.00–1.00 to 1.00. Pure titanium dioxide and zinc oxide as reference materials were also tested.

3.1. Hydrogen

Hydrogen itself is a desired product of the photochemical decomposition of water. It is also an intermediate product necessary for the photochemical decomposition of CO₂ into other valuable compounds. When irradiated with UV-Vis radiation, it is formed in the process of water splitting. Fig. 6 shows the graphs of the increase in the amount of hydrogen during the process for a group of materials containing TiO₂.

The amount of hydrogen generated after 6 h of the process was in the range of 4.1–19.2 $\mu\text{mol/g}_{\text{material}}/\text{dm}^3$. The highest value was observed for the 0.05 CS/TiO₂ sample and the lowest for the 0.50 CS/TiO₂ material. Only one of the five tested mixtures was characterized by higher hydrogen production activity compared to pure TiO₂, and that was the 0.05 CS/TiO₂ sample. In addition, hydrogen could not be detected for most samples until the second hour of the process. The graph shows fluctuations in the content of this component and even a decrease in its amount (e.g. for the sample 1.00 CS/TiO₂ – from 10.4 $\mu\text{mol/g}_{\text{material}}/\text{dm}^3$ after 4 h of the process to 7.8 $\mu\text{mol/g}_{\text{material}}/\text{dm}^3$ after 6 h). This can be explained by the fact that hydrogen in the CO₂ reduction process is an intermediate product continuously consumed in the reactions to form CO and CH₄.

No correlation was observed between the addition of carbon spheres and the amount of hydrogen produced. It can only be said that a small addition of carbon spheres (0.05 g of CS per 1 g of TiO₂) improved the photocatalytic properties of TiO₂ for hydrogen production. However, the further addition of carbon spheres negatively impacted the amount of H₂ produced.

Fig. 7 shows analogous diagrams for hydrogen production with ZnO as the active phase. In this case, slightly less hydrogen was obtained. It was in the range of 2.8–14.0 $\mu\text{mol/g}_{\text{material}}/\text{dm}^3$. In contrast to CS/TiO₂, the highest result was obtained for the sample with the highest addition of carbon spheres – 1.00 CS/ZnO, and at the same time it was the only material whose use resulted in the production of hydrogen at a level close to that of pure ZnO. In addition, a more significant effect of adding carbon spheres on H₂ production can be observed here. The hydrogen content decreased significantly at low CS additions, and it began to increase at the addition of ≥ 0.25 g of CS per 1 g of ZnO. Variations in the

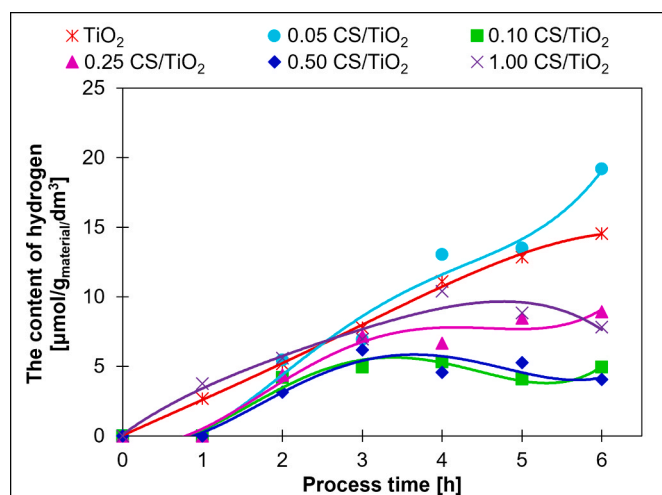


Fig. 6. The total content of H₂ in the gas phase after 6 h of the process with various CS/TiO₂ photocatalysts.

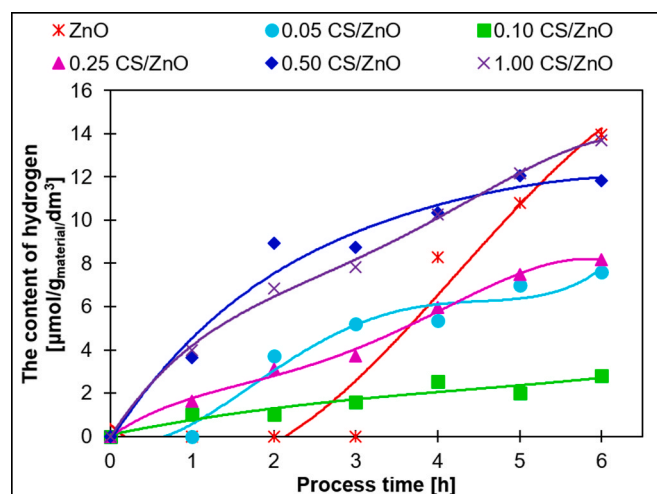


Fig. 7. The total content of H₂ in the gas phase after 6 h of the process with various CS/ZnO photocatalysts.

amount of this component can also be observed during the process. It is important to note that small amounts of hydrogen could already be detected after 1 h of the process in the tests with materials containing carbon spheres. At the same time, with pure ZnO it was visible on the chromatogram only after 4 h. Thus, it can be said that the addition of carbon spheres accelerates the process of hydrogen generation, but does not increase its amount.

Comparing the two groups of tested materials, it can be concluded that the amounts of hydrogen obtained were in a similar range, regardless of the active phase used. The addition of carbon spheres did not improve the photocatalytic properties of the materials for hydrogen production. Nevertheless, more favorable results were obtained for TiO₂ at a deficient CS concentration in the sample. On the other hand, for the ZnO samples, the highest amount of hydrogen was observed using the material with the highest percentage of carbon spheres tested.

A graph comparing the H₂ production after 6 h as a function of the number of carbon spheres for both tested groups is presented in Fig. 8. As mentioned earlier, in the presence of carbon dioxide, the hydrogen produced is consumed by producing carbon monoxide and methane. Therefore, photocatalysts used for a photocatalytic reduction of CO₂ should not be evaluated based on the amount of hydrogen produced.

3.2. Carbon monoxide

Carbon monoxide can be produced directly during the carbon

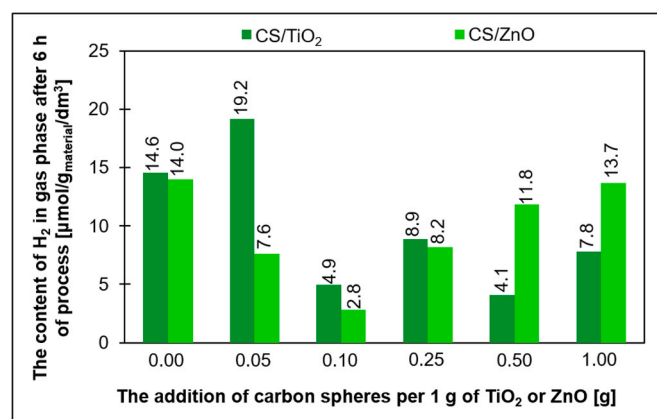


Fig. 8. The dependence of the amount of hydrogen after 6 h of process on the addition of carbon spheres for CS/TiO₂ and CS/ZnO materials.

dioxide reduction according to the reaction (3). At the same time, it can be a product of methane oxidation in reactions that take place under UV radiation [70]:



Under the conditions used in the experiments described in Section 2.5., carbon monoxide is the main product of the process. The graphs of the CO content in the gas phase for the subsequent CS/TiO₂ are shown in Fig. 9. It can be concluded that the addition of carbon spheres positively affected the production of carbon monoxide. For all tested mixtures of titanium dioxide with carbon spheres, the produced volumes of carbon monoxide were higher compared to pure TiO₂. The highest CO volume was obtained using 0.10 CS/TiO₂ material, and it was 19.3 μmol/g_{material}/dm³ after 6 h of the process. Further additions of carbon spheres caused a decrease of carbon monoxide content in the gas phase to 11.5 μmol/g_{material}/dm³ after 6 h of the process for the material with the highest CS addition (1.00 CS/TiO₂). For pure TiO₂, it was only 10.7 μmol/g_{material}/dm³. It is also important to note that the amount of carbon monoxide increased linearly at different rates for all processes. The presence of CO in the gas phase was observed already after 1 h of the process. This fact allows us to conclude that the reduction of CO₂ began immediately after the irradiation started, and the addition of carbon spheres additionally accelerated this process, as evidenced by the higher amounts of CO obtained in tests with CS/TiO₂ mixtures.

In the case of materials containing ZnO, the amounts of obtained CO were in the range of 7.0–15.9 μmol/g_{material}/dm³, as presented in Fig. 10. The highest result was noted for pure ZnO. Unlike for TiO₂, the addition of carbon spheres did not improve the photocatalytic properties of zinc oxide. It is interesting, however, that with the addition of carbon spheres between 0.05 and 0.25 g of CS per 1 g of ZnO, the carbon monoxide content decreased and then increased at higher CS contents in the samples. The highest result among the CS/ZnO mixtures was recorded for 1.00 CS/ZnO material, and it was 13.3 μmol/g_{material}/dm³ after 6 h of process. Based on the results, it can be concluded that a higher addition of CS to ZnO is more advantageous, but it generally reduces the photoactivity of zinc oxide.

Comparing both groups of tested materials (Fig. 11), it can be assumed that similar amounts of carbon monoxide were produced in performed processes, although the tests using TiO₂-containing materials yielded slightly higher results. The most preferred amount of carbon spheres to TiO₂ was 0.10 g per 1 g of TiO₂. In turn, for ZnO, it was 1.00 g of CS per 1 g. However, it should be noted that despite that fact, a lower

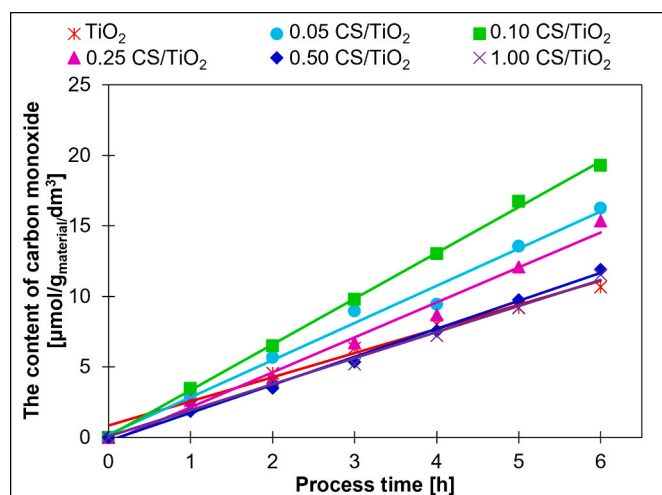


Fig. 9. The total content of CO in the gas phase after 6 h of the process with various CS/TiO₂ photocatalysts.

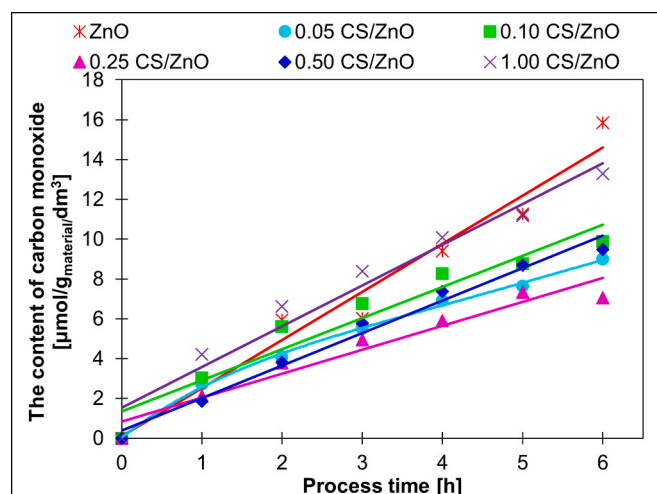


Fig. 10. The total content of CO in the gas phase after 6 h of the process with various CS/ZnO photocatalysts.

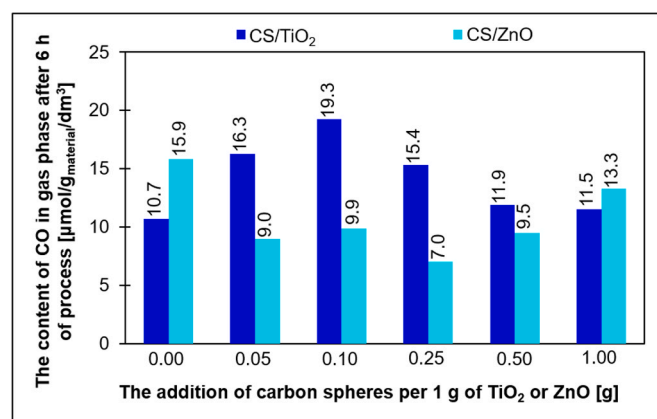


Fig. 11. The dependence of the amount of carbon monoxide after 6 h of process on the addition of carbon spheres for CS/TiO₂ and CS/ZnO materials.

result was obtained for this material compared to pure ZnO.

3.3. Methane

Methane is the last of the analysed products of the photocatalytic reduction of carbon dioxide. The production of this compound requires 8 electrons (Eq. (4)), which is why this reaction is the most difficult to perform. The energy and electrons present in the reactor are constantly involved in competing reactions. Additionally, methane molecules may undergo oxidation, as mentioned in Section 3.2.

In processes using CS/TiO₂ materials, small amounts of methane were obtained (0.4–0.6 μmol/g_{material}/dm³), as presented in Fig. 12. Moreover, no correlation was revealed between the amount of produced CH₄ and the number of carbon spheres in the samples. Regardless of this, similar values of this compound were obtained.

Conclusions may be slightly different in the case of materials containing ZnO. Although the amounts of methane produced were also negligible, adding 1.00 g of CS to 1 g of ZnO increased methane production to 1.7 μmol/g_{material}/dm³. For pure ZnO, it was only 0.5 μmol/g_{material}/dm³. The summary graph for the group of CS/ZnO materials is shown in Fig. 13. Fig. 14 compares the amount of methane obtained after 6 h of the process for both groups of materials.

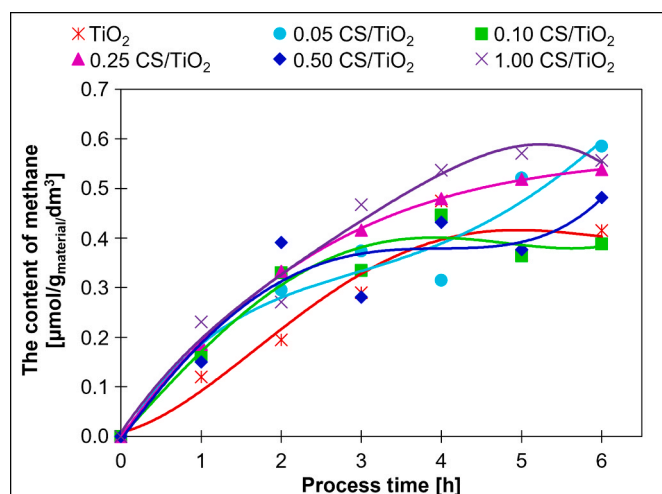


Fig. 12. The total content of CH₄ in the gas phase after 6 h of the process with various CS/TiO₂ photocatalysts.

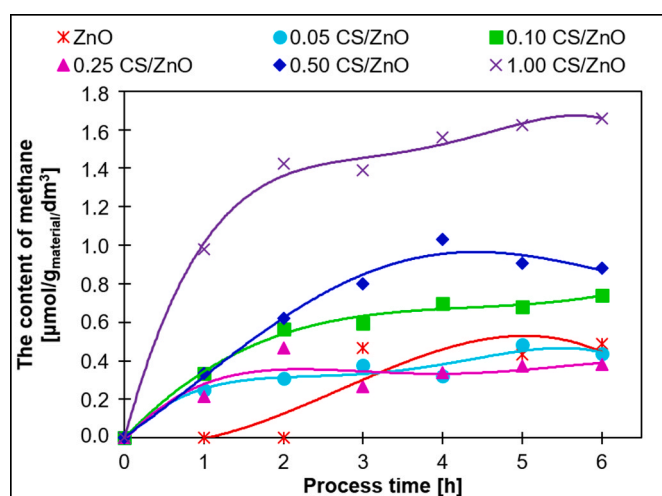


Fig. 13. The total content of CH₄ in the gas phase after 6 h of the process with various CS/ZnO photocatalysts.

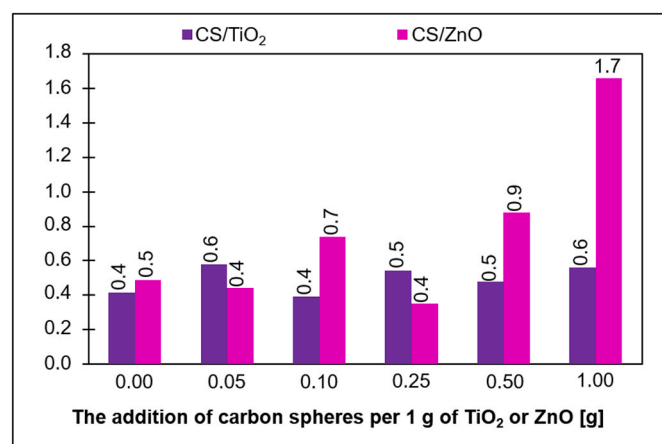


Fig. 14. The dependence of the amount of methane after 6 h of process on the addition of carbon spheres for CS/TiO₂ and CS/ZnO materials.

4. Conclusions

The experiments were carried out to evaluate the photocatalytic activity of two groups of materials containing TiO₂ and ZnO with the addition of carbon spheres in the amount of 0.05–1.00 g of CS per 1 g of TiO₂/ZnO in CO₂ reduction. These processes were performed in the liquid phase using 0.2 M NaOH aqueous solution. The samples were irradiated with UV-Vis light for 6 h.

Hydrogen, carbon monoxide, and methane products have been identified in the gas phase. The results were compared with those for initial materials, i.e. pure TiO₂ and ZnO. Based on the results, it can be concluded that both groups of materials generated similar amounts of the products mentioned above. However, samples containing TiO₂ had slightly higher activity in hydrogen and carbon monoxide production than ZnO-containing materials. On the other hand, more methane was produced in the processes using CS/ZnO samples, although it was an insignificant amount for all the tested samples.

The main product of the performed processes was carbon monoxide. Similar amounts of hydrogen were also obtained, although, in the reduction of CO₂, it was an intermediate product, constantly consumed in the reactions leading to the formation of CO and CH₄. It can also be assumed that adding carbon spheres to titanium dioxide improved its photocatalytic properties in the production of carbon monoxide. In the case of CS/ZnO materials, no increase in activity was observed.

Based on the results, it can be concluded that a smaller amount of carbon spheres was more efficient for TiO₂-containing materials (0.10 g of CS per 1 g of P25), while for ZnO, better results were obtained with the sample containing the most significant amount of carbon spheres (1.00 g of CS per 1 g of ZnO). This discrepancy may indicate that intermolecular interactions occurring in the materials may have a greater influence on the CO₂ photoreduction process than the pore size distribution or increased CO₂ adsorption capacity. The less negative zeta potential of ZnO resulted in closer contact with the carbon sphere particles, giving better results for samples with a higher CS content. In turn, the higher activity of TiO₂ compared to ZnO could result from its higher S_{BET} and TPV values. Due to this fact, the contact time between the photocatalyst and the CO₂ molecule was longer. On the other hand, improved adsorption capacity provided by carbon spheres addition can at some point positively affect the photocatalyst performance. It should be noted that this will also depend on the photocatalytic ability of the active material itself.

CRediT authorship contribution statement

Antoni W. Morawski: Conceptualization, Methodology, Writing – original draft, Writing – review & editing, Supervision. **Katarzyna Cmiełowska:** Formal analysis, Investigation, Writing – original draft, Writing – review & editing, Visualization. **Ewelina Kusiak-Nejman:** Conceptualization, Methodology, Writing – review & editing, Supervision. **Piotr Staciwa:** Formal analysis, Investigation, Visualization. **Joanna Kapica-Kozar:** Formal analysis, Investigation. **Ewa Ekiert:** Formal analysis, Investigation. **Iwona Pelech:** Conceptualization, Methodology, Writing – review & editing, Supervision. **Urszula Nar-kiewicz:** Supervision, Funding acquisition.

Declaration of Competing Interest

The authors declare that they have no known competing financial interests or personal relationships that could have appeared to influence the work reported in this paper.

Data availability

No data was used for the research described in the article.

Acknowledgments

The research leading to these results has received funding from the Norway Grants 2014–2021 via the National Centre for Research and Development under the grant number NOR/POLNORCCS/PhotoRed/0007/2019-00.

References

- N.G. Moustakas, Strategic design and evaluation of metal oxides for photocatalytic CO₂ reduction, in: E.I. García-López, L. Palmisano (Eds.), *Materials Science in Photocatalysis*, Elsevier, 2021, pp. 255–265, <https://doi.org/10.1016/C2019-0-03657-6>.
- T. Ochiai, A. Fujishima, Photoelectrochemical properties of TiO₂ photocatalyst and its application for environmental purification, *J. Photochem. Photobiol. C* 13 (4) (2012) 247–262, <https://doi.org/10.1016/j.jphotochemrev.2012.07.001>.
- U.I. Gaya, A.H. Abdullah, Heterogeneous photocatalytic degradation of organic contaminants over titanium dioxide: a review of fundamentals, progress and problems, *J. Photochem. Photobiol. C* 9 (1) (2008) 1–12, <https://doi.org/10.1016/j.jphotochemrev.2007.12.003>.
- T.P. Nguyen, D.L.T. Nguyen, V.H. Nguyen, T.H. Le, D.V.N. Vo, Q.T. Trinh, S.R. Bae, S.Y. Chae, S.Y. Kim, Q. Van Le, Recent advances in TiO₂-based photocatalysts for reduction of CO₂ to fuels, *Nanomaterials* 10 (2) (2020) 337, <https://doi.org/10.3390/nano10020337>.
- Q. Li, L. Jiang, Y. Li, X. Wang, L. Zhao, P. Huang, D. Chen, J. Wang, Enhancement of visible-light photocatalytic degradation of tetracycline by Co-doped TiO₂ templated by waste tobacco stem silk, *Molecules* 28 (1) (2023) 386, <https://doi.org/10.3390/molecules28010386>.
- L. Matejová, K. Kočí, M. Reli, L. Čapek, A. Hospodková, P. Peikertová, Z. Matěj, L. Obalová, A. Wach, P. Kuštrowski, A. Kotarba, Preparation, characterization and photocatalytic properties of cerium doped TiO₂: on the effect of Ce loading on the photocatalytic reduction of carbon dioxide, *Appl. Catal. B* 152–153 (2014) 172–183, <https://doi.org/10.1016/j.apcatb.2014.01.015>.
- T. Savchuk, I. Gavrilin, A. Savitskiy, A. Dronov, D. Dronova, S. Pereverzeva, A. Tarhanov, T. Maniecki, S. Gavrillov, E. Konstantinova, Effect of thermal treatment of symmetric TiO₂ nanotube arrays in argon on photocatalytic CO₂ conversion, *Symmetry* 14 (12) (2022) 2678, <https://doi.org/10.3390/sym14122678>.
- Q. Zhu, J. Qian, H. Pan, L. Tu, X. Zhou, Synergistic manipulation of micro-nanostructures and composition: anatase/rutile mixed-phase TiO₂ hollow micro-nanospheres with hierarchical mesopores for photovoltaic and photocatalytic applications, *Nanotechnology* 22 (39) (2011), 395703, <https://doi.org/10.1088/0957-4484/22/39/395703>.
- H. Zhao, L. Liu, J.M. Andino, Y. Li, Bicrystalline TiO₂ with controllable anatase–brookite phase content for enhanced CO₂ photoreduction to fuels, *J. Mater. Chem. A* 1 (28) (2013) 8209, <https://doi.org/10.1039/C3TA11226H>.
- L. Liu, H. Zhao, J.M. Andino, Y. Li, Photocatalytic CO₂ reduction with H₂O on TiO₂ Nanocrystals: comparison of anatase, rutile, and brookite polymorphs and exploration of surface chemistry, *ACS Catal.* 2 (8) (2012) 1817–1828, <https://doi.org/10.1021/cs300273q>.
- J.G. Li, T. Ishigaki, X. Sun, Anatase, brookite, and rutile nanocrystals via redox reactions under mild hydrothermal conditions: phase-selective synthesis and physicochemical properties, *J. Phys. Chem. C* 111 (13) (2007) 4969–4976, <https://doi.org/10.1021/jp0673258>.
- A. Di Paola, M. Bellardita, L. Palmisano, Brookite, the least known TiO₂ photocatalyst, *Catalysts* 3 (1) (2013) 36–73, <https://doi.org/10.3390/catal3010036>.
- P. Kar, S. Farsinezhad, N. Mahdi, Y. Zhang, U. Obuekwe, H. Sharma, J. Shen, N. Semagina, K. Shankar, Enhanced CH₄ yield by photocatalytic CO₂ reduction using TiO₂ nanotube arrays grafted with Au, Ru, and ZnPd nanoparticles, *Nano Res.* 9 (2016) 3478–3493, <https://doi.org/10.1007/s12274-016-1225-4>.
- J. Low, S. Qiu, D. Xu, C. Jiang, B. Cheng, Direct evidence and enhancement of surface plasmon resonance effect on Ag-loaded TiO₂ nanotube arrays for photocatalytic CO₂ reduction, *Appl. Surf. Sci.* 434 (2018) 423–432, <https://doi.org/10.1016/j.apsusc.2017.10.194>.
- Z. Jiang, X. Zhang, Z. Yuan, J. Chen, B. Huang, D.D. Dionysiou, G. Yang, Enhanced photocatalytic CO₂ reduction via the synergistic effect between Ag and activated carbon in TiO₂/AC-Ag ternary composite, *Chem. Eng. J.* 348 (2018) 592–598, <https://doi.org/10.1016/j.cej.2018.04.180>.
- M.S. Akple, J. Low, Z. Qin, S. Wageh, A.A. Al-Ghamdi, J. Yu, S. Liu, Nitrogen-doped TiO₂ microspheres with enhanced visible light photocatalytic activity for CO₂ reduction, *Chin. J. Catal.* 36 (12) (2015) 2127–2134, [https://doi.org/10.1016/S1872-2067\(15\)60989-5](https://doi.org/10.1016/S1872-2067(15)60989-5).
- Y. Sohn, W. Huang, F. Taghipour, Recent progress and perspectives in the photocatalytic CO₂ reduction of Ti-oxide-based nanomaterials, *Appl. Surf. Sci.* 396 (2017) 1696–1711, <https://doi.org/10.1016/j.apsusc.2016.11.240>.
- H. Deng, F. Xu, B. Cheng, J. Yu, W. Ho, Photocatalytic CO₂ reduction of C/ZnO nanofibers enhanced by an Ni-NiS Co-catalyst, *Nanoscale* 12 (13) (2020) 7206–7213, <https://doi.org/10.1039/c9nr10451h>.
- Y. Xu, C. Li, H. Huang, L. Huang, L. Peng, H. Pan, Hydrophobic functionalization of ZnO nanosheets by in situ center-substituted synthesis for selective photocatalysis under visible irradiation, *Part. Part. Syst. Charact.* 36 (3) (2019), 1800403, <https://doi.org/10.1002/ppsc.201800403>.
- S. Gao, W. Yang, J. Xiao, B. Li, Q. Li, Creation of passivated Nb/N p-n Co-doped ZnO nanoparticles and their enhanced photocatalytic performance under visible light illumination, *J. Mater. Sci. Technol.* 35 (4) (2019) 610–614, <https://doi.org/10.1016/j.jmst.2018.09.056>.
- H. Moussa, B. Chouchene, T. Gries, L. Balan, K. Mozet, G. Medjahdi, R. Schneider, Growth of ZnO nanorods on graphitic carbon nitride GCN sheets for the preparation of photocatalysts with high visible-light activity, *ChemCatChem* 10 (21) (2018) 4987–4997, <https://doi.org/10.1002/cctc.201801206>.
- S.G. Kumar, K.S.R. Koteswara Rao, Zinc oxide based photocatalysis: tailoring surface-bulk structure and related interfacial charge carrier dynamics for better environmental applications, *RSC Adv.* 5 (2015) 3306–3351, <https://doi.org/10.1039/c4ra13299h>.
- X. Zhang, J. Qin, Y. Xue, P. Yu, B. Zhang, L. Wang, R. Liu, Effect of aspect ratio and surface defects on the photocatalytic activity of ZnO nanorods, *Sci. Rep.* 4 (2014) 4–11, <https://doi.org/10.1038/srep04596>.
- A. McLaren, T. Valdes-Solis, G. Li, S.C. Tsang, Shape and size effects of ZnO nanocrystals on photocatalytic activity, *J. Am. Chem. Soc.* 131 (35) (2009) 12540–12541, <https://doi.org/10.1021/ja9052703>.
- G. Mano, S. Harinee, S. Sridhar, M. Ashok, A. Viswanathan, Microwave assisted synthesis of ZnO-PbS heterojunction for degradation of organic pollutants under visible light, *Sci. Rep.* 10 (2020) 2224, <https://doi.org/10.1038/s41598-020-59066-4>.
- G.T.S.T. da Silva, K.T.G. Carvalho, O.F. Lopes, E.S. Gomes, A.R. Malagutti, V. R. Mastelaro, C. Ribeiro, H.A.J.L. Mourão, Synthesis of ZnO nanoparticles assisted by N sources and their application in the photodegradation of organic contaminants, *ChemCatChem* 9 (19) (2017) 3795–3804, <https://doi.org/10.1002/cctc.201700756>.
- X. Liu, L. Ye, S. Liu, Y. Li, X. Ji, Photocatalytic reduction of CO₂ by ZnO micro/nanomaterials with different morphologies and ratios of {0001} facets, *Sci. Rep.* 6 (2016) 38474, <https://doi.org/10.1038/srep38474>.
- Y. Zhao, N. Liu, S. Zhou, J. Zhao, Two-dimensional ZnO for the selective photoreduction of CO₂, *J. Mater. Chem. A* 7 (27) (2019) 16294–16303, <https://doi.org/10.1039/C9TA04477A>.
- W. Luo, Q. Zhang, J. Zhang, E. Moiola, K. Zhao, A. Züttel, Electrochemical reconstruction of ZnO for selective reduction of CO₂ to CO, *Appl. Catal. B* 273 (2020), 119060, <https://doi.org/10.1016/j.apcatb.2020.119060>.
- H. Guzmán, F. Salomone, S. Bensaid, M. Castellino, N. Russo, S. Hernández, CO₂ conversion to alcohols over Cu/ZnO catalysts: prospective synergies between electrocatalytic and thermocatalytic routes, *ACS Appl. Mater. Interfaces* 14 (1) (2022) 517–530, <https://doi.org/10.1021/acami.1c15871>.
- D.L.T. Nguyen, M.S. Jee, D.H. Won, H. Jung, H.S. Oh, B.K. Min, Y.J. Hwang, Selective CO₂ reduction on zinc electrocatalyst: the effect of zinc oxidation state induced by pretreatment environment, *ACS Sustain. Chem. Eng.* 5 (12) (2017) 11377–11386, <https://doi.org/10.1021/acssuschemeng.7b02460>.
- W.A. Thompson, A. Olivo, D. Zanardo, G. Cruciani, F. Menegazzo, M. Signoretto, M.M. Maroto-Valer, Systematic study of TiO₂/ZnO mixed metal oxides for CO₂ photoreduction, *RSC Adv.* 9 (38) (2019) 21660–21666, <https://doi.org/10.1039/c9ra03435h>.
- F. Conte, E.I. García-López, G. Marci, C.L.M. Bianchi, G. Ramis, I. Rossetti, Carbon nitride-based catalysts for high pressure CO₂ photoreduction, *Catalysts* 12 (12) (2022) 1628, <https://doi.org/10.3390/catal12121628>.
- R. Liu, Z. Chen, Y. Yao, Y. Li, W.A. Cheema, D. Wang, S. Zhu, Recent advancements in G-C₃N₄-based photocatalysts for photocatalytic CO₂ reduction: a mini review, *RSC Adv.* 10 (49) (2020) 29408–29418, <https://doi.org/10.1039/d0ra05779g>.
- U. Ghosh, A. Majumdar, A. Pal, Photocatalytic CO₂ reduction over G-C₃N₄ based heterostructures: recent progress and prospects, *J. Environ. Chem. Eng.* 9 (1) (2021), 104631, <https://doi.org/10.1016/j.jece.2020.104631>.
- L. Zhang, L. Zhang, Y. Chen, Y. Zheng, J. Guo, S. Wan, S. Wang, C.K. Ngaw, J. Lin, Y. Wang, CdS/ZnO: a multipronged approach for efficient reduction of carbon dioxide under visible light irradiation, *ACS Sustain. Chem. Eng.* 8 (13) (2020) 5270–5277, <https://doi.org/10.1021/acssuschemeng.0c00190>.
- Y. Sun, Y. Han, X. Song, B. Huang, X. Ma, R. Xing, CdS/WO₃ S-scheme heterojunction with improved photocatalytic CO₂ reduction activity, *J. Photochem. Photobiol. B* 233 (2022), 112480, <https://doi.org/10.1016/j.jphotochem.2022.112480>.
- J. Wang, T. Xia, L. Wang, X. Zheng, Z. Qi, C. Gao, J. Zhu, Z. Li, H. Xu, Y. Xiong, Enabling visible-light-driven selective CO₂ reduction by doping quantum dots: trapping electrons and suppressing H₂ evolution, *Angew. Chem. Int. Ed.* 57 (50) (2018) 16447–16451, <https://doi.org/10.1002/anie.201810550>.
- B. Zhu, Q. Zhang, X. Li, H. Lan, Facile synthesis of ZnS/ZnO nanosheets with enhanced photocatalytic activity, *Phys. Status Solidi A* 215 (23) (2018), 1800359, <https://doi.org/10.1002/pssa.201800359>.
- F. Xu, B. Zhu, B. Cheng, J. Yu, J. Xu, 1D/2D TiO₂/MoS₂ hybrid nanostructures for enhanced photocatalytic CO₂ reduction, *Adv. Opt. Mater.* 6 (23) (2018) 8–15, <https://doi.org/10.1002/adom.201800911>.
- W. Tu, Y. Li, L. Kuai, Y. Zhou, Q. Xu, H. Li, X. Wang, M. Xiao, Z. Zou, Construction of unique two-dimensional MoS₂-TiO₂ hybrid nanojunctions: MoS₂ as a promising cost-effective cocatalyst toward improved photocatalytic reduction of CO₂ to methanol, *Nanoscale* 9 (2017) 065–070, <https://doi.org/10.1039/C7NR03238B>.
- M. Lv, H. Liu, Photocatalytic property and structural stability of CuAl-based layered double hydroxides, *J. Solid State Chem.* 227 (2015) 232–238, <https://doi.org/10.1016/j.jssc.2015.04.010>.
- G. Gao, Z. Zhu, J. Zheng, Z. Liu, Q. Wang, Y. Yan, Ultrathin magnetic Mg-Al LDH photocatalyst for enhanced CO₂ reduction: fabrication and mechanism, *J. Colloid Interface Sci.* 555 (1) (2019) 1–10, <https://doi.org/10.1016/j.jcis.2019.07.025>.

- [44] X. Wang, Z. Wang, Y. Bai, L. Tan, Y. Xu, X. Hao, J. Wang, A.H. Mahadi, Y. Zhao, L. Zheng, Y.-F. Song, Tuning the selectivity of photoreduction of CO₂ to syngas over Pd/layered double hydroxide nanosheets under visible light up to 600 nm, *J. Energy Chem.* 6 (2020) 1–7, <https://doi.org/10.1016/j.jechem.2019.10.004>.
- [45] A. Olivo, E. Ghedini, M. Signoretto, M. Compagnoni, I. Rossetti, Liquid vs. gas phase CO₂ photoreduction process: which is the effect of the reaction medium? *Energies* 10 (9) (2017) 1394, <https://doi.org/10.3390/en10091394>.
- [46] F. Galli, M. Compagnoni, D. Vitali, C. Pirola, C.L. Bianchi, A. Villa, L. Prati, I. Rossetti, CO₂ photoreduction at high pressure to both gas and liquid products over titanium dioxide, *Appl. Catal. B* 200 (2017) 386–391, <https://doi.org/10.1016/j.apcatb.2016.07.038>.
- [47] O. Ola, M.M. Maroto-Valer, Review of material design and reactor engineering on TiO₂ photocatalysis for CO₂ reduction, *J. Photochem. Photobiol. C* 24 (2015) 16–42, <https://doi.org/10.1016/j.jphotochemrev.2015.06.001>.
- [48] C.C. Lo, C.H. Hung, C.S. Yuan, J.F. Wu, Photoreduction of carbon dioxide with H₂ and H₂O over TiO₂ and ZrO₂ in a circulated photocatalytic reactor, *Sol. Energy Mater. Sol. Cells* 91 (19) (2007) 1765–1774, <https://doi.org/10.1016/j.solmat.2007.06.003>.
- [49] K. Niu, Y. Xu, H. Wang, R. Ye, H.L. Xin, F. Lin, C. Tian, Y. Lum, K.C. Bustillo, M. M. Doeff, M.T.M. Koper, J. Ager, R. Xu, H. Zheng, A spongy nickel-organic CO₂ reduction photocatalyst for nearly 100% selective CO production, *Sci. Adv.* 3 (7) (2017), e1700921, <https://doi.org/10.1126/sciadv.1700921>.
- [50] Y. Tavan, S.H. Hosseini, A novel rate of the reaction between NaOH with CO₂ at low temperature in spray dryer, *Petroleum* 3 (1) (2017) 51–55, <https://doi.org/10.1016/j.petlm.2016.11.006>.
- [51] J.K. Stolaroff, D.W. Keith, G.V. Lowry, Carbon dioxide capture from atmospheric air using sodium hydroxide spray, *Environ. Sci. Technol.* 42 (8) (2008) 2728–2735, <https://doi.org/10.1021/es702607w>.
- [52] L. Trisnaliani, D.E. Pranata, Patria, Tahdid, K.A. Ridwan, M.N. Alfarizi, M. P. Lumbantoran, The effect of flowrate and NaOH concentration to CO₂ reduction in biogas products using absorber, *J. Phys. Conf. Ser.* 1500 (2020), 012054, <https://doi.org/10.1088/1742-6596/1500/1/012054>.
- [53] M. Yoo, S.-J. Han, J.-H. Wee, Carbon dioxide capture capacity of sodium hydroxide aqueous solution, *J. Environ. Manag.* 114 (2013) 512–519, <https://doi.org/10.1016/j.jenvman.2012.10.061>.
- [54] C. Dasaard, D.J. Bayless, B.J. Stuart, Saturated pH and total inorganic carbon from CO₂ solubility related to algal growth, *Int. Adv. Res. J. Sci. Eng. Technol.* 3 (11) (2016) 146–150, <https://doi.org/10.17148/iarjset.2016.31128>.
- [55] K. Kočí, L. Obalová, L. Matějová, D. Plachá, Z. Lačný, J. Jirkovský, O. Šolcová, Effect of TiO₂ particle size on the photocatalytic reduction of CO₂, *Appl. Catal. B* 89 (3–4) (2009) 494–502, <https://doi.org/10.1016/j.apcatb.2009.01.010>.
- [56] A.W. Morawski, E. Kusiak-Nejman, I. Pelech, K. Ćmiełowska, D. Sibera, P. Staciwa, A. Wanag, M. Gano, E. Ekiert, J. Kapica-Kozar, K. Witkowski, U. Narkiewicz, New insight on carbon dioxide-mediated hydrogen production, *ChemistryOpen* 11 (4) (2022), e202100262, <https://doi.org/10.1002/open.202100262>.
- [57] P. Liu, X. Peng, Y.-L. Men, Y.-X. Pan, Recent progresses on improving CO₂ adsorption and proton production for enhancing efficiency of photocatalytic CO₂ reduction by H₂O, *Green Chem. Eng.* 1 (1) (2020) 33–39, <https://doi.org/10.1016/j.gce.2020.09.003>.
- [58] I. Pelech, D. Sibera, P. Staciwa, E. Kusiak-Nejman, J. Kapica-Kozar, A. Wanag, U. Narkiewicz, A.W. Morawski, ZnO/carbon spheres with excellent regenerability for post-combustion CO₂ capture, *Materials* 14 (21) (2021) 6478, <https://doi.org/10.3390/ma14216478>.
- [59] I. Pelech, E. Kusiak-Nejman, P. Staciwa, D. Sibera, J. Kapica-Kozar, A. Wanag, F. Latzke, K. Pawłowska, A. Michalska, U. Narkiewicz, A.W. Morawski, CO₂ sorbents based on spherical carbon and photoactive metal oxides: insight into adsorption capacity, selectivity and regenerability, *Molecules* 27 (20) (2022) 6802, <https://doi.org/10.3390/molecules27206802>.
- [60] I. Pelech, D. Sibera, P. Staciwa, E. Kusiak-Nejman, J. Kapica-Kozar, A. Wanag, U. Narkiewicz, A.W. Morawski, ZnO/carbon spheres with excellent regenerability for post-combustion CO₂ capture, *Materials* 14 (21) (2021) 6478, <https://doi.org/10.3390/ma14216478>.
- [61] I. Pelech, P. Staciwa, D. Sibera, E. Kusiak-Nejman, A.W. Morawski, J. Kapica-Kozar, U. Narkiewicz, The effect of the modification of carbon spheres with ZnCl₂ on the adsorption properties towards CO₂, *Molecules* 27 (4) (2022) 1387, <https://doi.org/10.3390/molecules27041387>.
- [62] I. Pelech, D. Sibera, P. Staciwa, U. Narkiewicz, R. Cormia, Pressureless and low-pressure synthesis of microporous carbon spheres applied to CO₂ adsorption, *Molecules* 25 (22) (2020) 5328, <https://doi.org/10.3390/molecules25225328>.
- [63] M.E. Casco, M. Martínez-Escandell, J. Silvestre-Albero, F. Rodríguez-Reinoso, Effect of the porous structure in carbon materials for CO₂ capture at atmospheric and high-pressure, *Carbon* 67 (2014) 230–235, <https://doi.org/10.1016/j.carbon.2013.09.086>.
- [64] N.P. Wickramaratne, M. Jaroniec, Importance of small micropores in CO₂ capture by phenolic resin-based activated carbon spheres, *J. Mater. Chem. A* 1 (2013) 112–116, <https://doi.org/10.1039/C2TA00388K>.
- [65] L.K.C. De Souza, N.P. Wickramaratne, A.S. Ello, M.J.F. Costa, C.E.F. Da Costa, M. Jaroniec, Enhancement of CO₂ adsorption on phenolic resin-based mesoporous carbons by KOH activation, *Carbon* 5 (2013) 334–340, <https://doi.org/10.1016/j.carbon.2013.08.034>.
- [66] K.S. Sobczuk, I. Pelech, U. Narkiewicz, P. Staciwa, D. Sibera, D. Moszyński, The influence of the synthesis pH on the morphology and adsorption properties of carbon spheres, *Appl. Surf. Sci.* 608 (2023), 155196, <https://doi.org/10.1016/j.apsusc.2022.155196>.
- [67] Z. Wang, J. Hong, S.F. Ng, W. Liu, J. Huang, P. Chen, W.J. Ong, Recent progress of perovskite oxide in emerging photocatalysis landscape: water splitting, CO₂ reduction, and N₂ fixation, *Acta Phys. Chim. Sin.* 37 (6) (2021), 2011033, <https://doi.org/10.3866/PKU.WHXB202011033>.
- [68] P. Wang, G. Yin, Q. Bi, X. Huang, X. Du, W. Zhao, F. Huang, Efficient photocatalytic reduction of CO₂ using carbon-doped amorphous titanium oxide, *ChemCatChem* 10 (17) (2018) 3854–3861, <https://doi.org/10.1002/CCTC.201800476>.
- [69] M. Tasbihi, K. Kočí, I. Troppová, M. Edelmánová, M. Reli, L. Čapek, R. Schomäcker, Photocatalytic reduction of carbon dioxide over Cu/TiO₂ photocatalysts, *Environ. Sci. Pollut. Res.* 25 (2018) 34903–34911, <https://doi.org/10.1007/S11356-017-0944-8>.
- [70] X. Yu, V. De Waele, A. Löfberg, V. Ordonsky, A.Y. Khodakov, Selective photocatalytic conversion of methane into carbon monoxide over zinc-heteropolyacid-titania nanocomposites, *Nat. Commun.* 10 (2019) 700, <https://doi.org/10.1038/s41467-019-08525-2>.